Advances in Applied Mathematics and Mechanics
Adv. Appl. Math. Mech., Vol. **9**, No. 1, pp. 205-232

DOI: 10.4208/aamm.2016.m1479
February 2017

# Similarity Solution for the Synchronous Grouting of Shield Tunnel Under the Vertical Non-Axisymmetric Displacement Boundary Condition

Jinfeng Zou[1,*] and Songqing Zuo[2]

[1] *School of Civil Engineering, Central South University, Changsha, Hunan 410083, China*
[2] *School of Civil Engineering, Central South University Railway Campus, Changsha, Hunan 410075, China*

Received 3 March 2016; Accepted (in revised version) 29 August 2016

**Abstract.** Similarity solution is investigated for the synchronous grouting of shield tunnel under the vertical non-axisymmetric displacement boundary condition in the paper. The synchronous grouting process of shield tunnel was simplified as the cylindrical expansion problem, which was based on the mechanism between the slurry and stratum of the synchronous grouting. The stress harmonic function on the horizontal and vertical ground surfaces is improved. Based on the virtual image technique, stress function solutions and Boussinesq's solution, elastic solution under the vertical non-axisymmetric displacement boundary condition on the vertical surface was proposed for synchronous grouting problems of shield tunnel. In addition, the maximum grouting pressure was also obtained to control the vertical displacement of horizontal ground surface. The validity of the proposed approach was proved by the numerical method. It can be known from the parameter analysis that larger vertical displacement of the horizontal ground surface was induced by smaller tunnel depth, smaller tunnel excavation radius, shorter limb distance, larger expansion pressure and smaller elastic modulus of soils.

**AMS subject classifications**: 74G15, 74A10, 74Bxx

**Key words**: Vertical non-axisymmetric displacement boundary, stresses and displacements, virtual image technique, cylindrical cavity expansion source, image source, stress harmonic function, shield tunnel, synchronous grouting, maximum grouting pressure.

## 1 Introduction

Construction method of shield tunnel was apprehensively applied to the city highway, underground subway, drainage, power and communication facilities due to the fatly and

*Corresponding author.
*Email:* zoujinfeng_csu@163.com (J. F. Zou), zsq2011510409@163.com (S. Q. Zuo)

 

safety construction and the small influences on the surrounding environment. Because of the tunnel excavation technique, the ground movement caused by the shield tunnel excavation can't be completely eliminated no matter how the shield tunnel construction technique is improved. When a ground displacement take place in the construction process of shield tunnel, surface depositing, structures leaning or dumping will be appear, especially in the non-axisymmetric displacement boundary condition on the vertical surface. However, synchronous grouting technique can improve the stability of the surrounding rock and control the ground surface deformation in the shield tunnel construction process.

For the prediction method of the ground settlement caused by shield construction, many literatures and results have been published with the empirical formula, theoretical analytical method, model test, neural network, stochastic medium theory and numerical calculation, etc. For example, Peck [2] proposed an empirical formula for predicting the ground settlement during the tunnel opening based on the monitoring results. Wood [3] pointed out that the ground loss is the main effective factors of the tunnel excavating in soft soil mass. A cumulative probability curve formula was proposed by Attewell and Woodman [5] to predict the vertical ground settlement at the axil of tunnel in soil mass. Sagaseta [6] proposed the analytic solution of three-dimensional surface deformation for the undrained soil deformation due to the ground loss in elastic semi-infinite space. Rowe and Lee [8, 9] pointed out that the gap parameter would have significant effects on the vertical displacement and the magnitude of ground loss during the tunnel opening in the soft soil. Verruijt and Booker [10] proposed the prediction approach of the ground settlements due to deformation of a tunnel in an elastic half plane. Based on the Peck formula and a large number of local experiments, Loganathan and Poulos [11] proposed an analytical prediction technique for tunneling-induced ground movement in clays. Swoboda and Abu-Krisha [12] presented a new field to analyze three-dimensional (3-D) coupled linear flow for Tunnel Boring Machine (TBM) tunnelling in saturated porous medium. Loganathan et al. [13] carried out three centrifuge model tests to assess tunneling-induced ground deformations in clays and their effects on adjacent pile foundations. The specified ground loss values were achieved by reducing the diameter of the model tunnel and designed to simulate the two-dimensional tunnel-induced ground movements. Berg Van der et al. [14] summed up the transverse and longitudinal ground settlement law by the Heathrow fast tunnel deformation monitoring. Li et al. [15] obtained the elastic solution of the spherical cavity expansion under the inclined non-axisymmetric displacement boundary condition, by using coordinate transformation. Zou and Li [17], Zou and He [18], Zou et al. [19], Zou and Su [20] developed the prediction approaches of stress and displacement incorporating the effects of seepage force, hydraulic-coupling, and out-of-planes stress. Zou and Zuo [21] investigated approximate solution of the cylindrical cavity expansion under the inclined non-axisymmetric displacement boundary condition.

Therefore, it can be known that the above researches of the ground surface settlement mainly focused on the empirical method and the numerical method. Moreover,

it is relatively weak for the works based on the method of the elasticity theory, especially for the stratum deformation caused by synchronous grouting under the vertical non-axisymmetric boundary condition in the practical engineering.

Based on the above reasons, the stratum effect caused by the synchronous grouting of shield tunnel under the non-axisymmetric boundary condition on the vertical surface is investigated. At first, the virtual image technique [6] was adopted to revise the shear stress on the vertical surface to be zero. Then, the modified stress harmonic function is applied to revise vertical normal stress and shear stress of the ground surface to be zero, the Boussinesq's solution [1] is adopted to balance the horizontal normal stress on the vertical surface. Using the linear elastic superposition principle, the elastic solution is obtained for synchronous grouting problems of shield tunnel under the vertical non-axisymmetric displacement boundary condition. Moreover, the prediction formula of the maximum grouting pressure was developed based on the proposed approach for the synchronous grouting of shallow buried shield tunnels. The numerical validation was carried out to validate the correctness of the proposed approach. Finally, some important conclusions are acquired by the numerical analysis and discussion.

## 2 Theory and methodology

### 2.1 Problem description

Generally speaking, the action of synchronous grouting on the surrounding soil is mostly compaction in soft clay soil and permeability in sand if the grouting pressure is reasonable. The additional radial pressure is produced in the surrounding soil by compaction or permeability effectiveness. Therefore, the action of the additional radial pressure on the surrounding soil is considered as the cylindrical cavity expansion problem.

As shown in Fig. 1, synchronous grouting of shield tunnel on the soil stratum can be simplified as the cylindrical expansion problem under the vertical non-axisymmetric boundary condition. Taking the intersection point $o$ of the horizontal ground surface and vertical surface as the origin point, the $x$ axis, $z$ axis and $y$ axis as the positive directions, the space rectangular coordinate system is established. The initial radius of the cylindrical cavity is $r_0$, which is about equal to shield tunnel excavation radius. The buried depth of the cylindrical cavity is $h$, which is about equal to shield tunnel depths. The limb distance from the cylindrical cavity to the vertical ground surface is $t$. The internal expansion pressure of the cylindrical cavity is $p$, which is the difference value between grouting pressure and initial soil hydrostatic pressure. The distance between the cylindrical cavity center $o_1$ and the calculation point $q(x,0,z)$ is $R$. The free vertical and horizontal ground surface boundary are located at the position (i.e., $x=0$ and $z=0$).

### 2.2 Assumption

In order to simplify the engineering practice and obtain the elastic solution in synchrono-

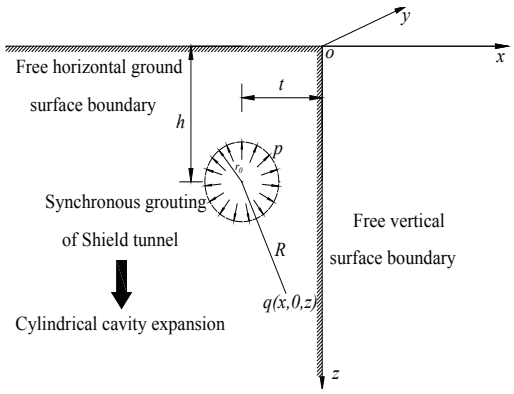


Figure 1: Synchronous grouting of shield tunnel under the vertical non-axisymmetric displacement boundary condition.

us grouting of shield tunneling under the vertical non-axisymmetric displacement boundary condition, the following assumptions are adopted:

(1) Soil mass is homogeneous and isotropic, which satisfies the linear elastic, Hooke's law and small deformation;

(2) The ground surface is flat. The weight of soil mass and the initial earth stress are ignored, and soil mass cannot be compressed ($v=0.5$);

(3) The stratum action resulting from synchronous grouting of shield tunnel can be simplified as the cylindrical cavity expansion problem;

(4) A uniform annular clearance is formed behind the shield machine tail after the segment is divorced from the shield machine tail, shown in Fig. 2.

(5) The shield tail is filled with the grout and imposed on the surrounding strata, and the uniform radial expansion pressure is equal to the difference value between grouting pressure and initial water and soil pressure;

(6) Soil mass will bear the compaction effect. The soil deformation occurs instantly after the grout filling the shield tail clearance and the time effect of grout properties and soil deformation are not considered.

(7) The effect of the vertical normal stress and shear stress correction of the horizontal ground surface on the vertical ground surface is not considered in the calculation of displacements and stresses.

## 2.3 Research idea

Elastic solutions of displacement and stress for cylindrical cavity expansion problems under the vertical non-axisymmetric displacement boundary condition are solved based on the virtual image technique [6], stress function method [4] and Boussisq's solutions [1].

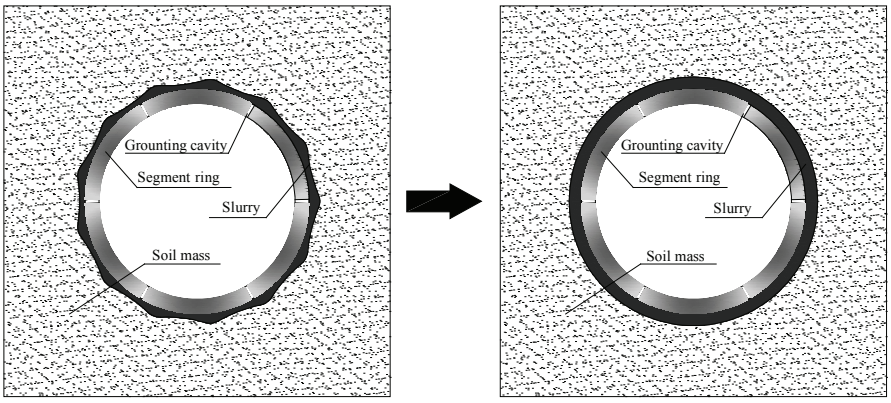


(a) Non-uniform shield tail clearance (b) Uniform shield tail clearance

Figure 2: Generalized sketch of shield tail clearance.

The horizontal ground surface and vertical surface boundaries won't satisfy the free displacement boundary condition under the combined action of the cylindrical cavity expansion source and image source. As a consequence, the stresses of the ground and vertical surface boundaries all need to be revised by following approaches.

The stress correction method is that an equivalent distributed force with the opposite direction is applied to the corresponding boundary, and the specific approaches are as follows:

(1) When the horizontal ground surface and vertical surface boundaries are not considered, elastic solutions of stress and displacement for the cylindrical cavity expansion in infinite space are obtained under the combined action of the cylindrical cavity expansion source and image source;

(2) The stress function method is adopted to carry out the first correction for the vertical normal stress in the ground surface which is generated by the combined action of the cylindrical cavity expansion source and image source;

(3) The stress function method is also adopted to carry out the second correction for shear stress on the ground surface which is generated by he combined action of the cylindrical cavity expansion source and image source;

(4) The horizontal normal stress on the vertical surface boundary is corrected through the integration of Boussinesq's solution and coordinate transformation formula;

(5) Elastic solutions of stress and displacement are obtained by the linear superposition from Step (1) to Step (4) under the vertical non-symmetric displacement boundary condition.

## 2.4 Elastic solution

### 2.4.1 Elastic solution before correction

Fig. 3 shows the mechanical model of cylindrical cavity expansion under the vertical non-axisymmetric displacement boundary condition. The cylindrical cavity expansion source $o_1$ will be described with the initial radius $r_0$, the cylindrical cavity depth $h$, the limb distance $t$, the internal expansion pressure $p$. The free vertical surface boundary is located at the position (i.e., $x=0$) and the free horizontal ground surface boundary is located at the position (i.e., $z=0$). Taking free vertical ground surface boundary as the mirror image symmetry, the image source $o_2$ is set in the corresponding position. $R_1$ is the distance between the center of cylindrical cavity expansion source $o_1$ and the calculation point $q(x,0,z)$, $R_2$ is the distance between the center of image source $o_2$ and the calculation point $q(x,0,z)$.

According to the geometric relations in Fig. 3, $R_1$ and $R_2$ are given by

$$\begin{cases} R_1=\sqrt{|qo_4|^2+|o_1o_4|^2}=\sqrt{(x+t)^2+(z-h)^2}, \\ R_2=\sqrt{|qo_3|^2+|o_2o_3|^2}=\sqrt{(x-t)^2+(z-h)^2}. \end{cases} \tag{2.1}$$

Based on the fundamental elastic mechanics theory (Davis and Selvadurai, 1988), the elastic solutions of the cylindrical cavity expansion problem in the infinite space can be expressed in polar coordinates as follows (the tensile stress is positive and the outward

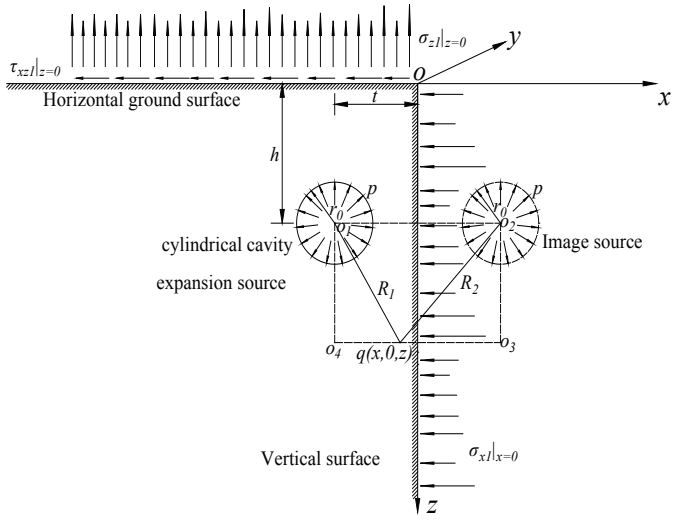


Figure 3: Stresses caused by the cylindrical cavity expansion under the vertical non-asymmetry displacement boundary condition.

radial displacement is positive):

$$\sigma_{R1}=-\frac{p{r_0}^2}{{R_1}^2}, \tag{2.2a}$$

$$\sigma_{\theta 1}=\frac{p{r_0}^2}{{R_1}^2}, \tag{2.2b}$$

$$\tau_{R\theta 1}=0, \tag{2.2c}$$

$$U_{R1}=\frac{(1+v)pR_1}{E}\left(\frac{r_0}{R_1}\right)^2=\frac{p{r_0}^2}{2GR_1}, \tag{2.2d}$$

where, $\sigma_{R1}$, $\sigma_{\theta 1}$, $\tau_{R\theta 1}$, $U_{R1}$ are the radial normal stress, the circumferential normal stress, shear stress and the radial displacement at the point $q(R_1,0,\theta_1)$ produced by the cylindrical cavity expansion source in the infinite space, respectively;

$$\sigma_{R2}=-\frac{p{r_0}^2}{{R_2}^2}, \tag{2.3a}$$

$$\sigma_{\theta 2}=\frac{p{r_0}^2}{{R_2}^2}, \tag{2.3b}$$

$$\tau_{R\theta 2}=0, \tag{2.3c}$$

$$U_{R2}=\frac{(1+v)pR_2}{E}\left(\frac{r_0}{R_2}\right)^2=\frac{p{r_0}^2}{2GR_2}, \tag{2.3d}$$

where, $\sigma_{R2}$, $\sigma_{\theta 2}$, $\tau_{R\theta 2}$, $U_{R2}$ are the radial normal stress, circumferential normal stress, shear stress and radial displacement at the point $q(R_2,0,\theta_2)$ produced by the image source in the infinite space, respectively.

Because the stress and displacement of the soil mass is studied in the $xoz$ plane, it is necessary to adopt the coordinate transformation formula of the stresses and displacements in elastic mechanics [7]. The coordinate transformation formula of cylindrical cavity expansion in the infinite space are as follows:

$$U_x=U_R\cos\theta, \tag{2.4a}$$

$$U_z=U_R\sin\theta, \tag{2.4b}$$

$$\sigma_x=\sigma_R\cos^2\theta+\sigma_\theta\sin^2\theta-\tau_{R\theta}\sin 2\theta, \tag{2.4c}$$

$$\sigma_z=\sigma_R\sin^2\theta+\sigma_\theta\cos^2\theta+\tau_{R\theta}\sin 2\theta, \tag{2.4d}$$

$$\tau_{xz}=(\sigma_R-\sigma_\theta)\sin\theta\cos\theta+\tau_{R\theta}\cos 2\theta, \tag{2.4e}$$

where, $U_x$, $U_z$, $\sigma_x$, $\sigma_z$ and $\tau_{xz}$ are the horizontal displacement, vertical displacement, horizontal normal stress, vertical normal stress and shear stress at the point $q(x,0,z)$ of the plane rectangular coordinate system in the infinite soil mass, respectively; $U_R$, $\sigma_R$, $\sigma_\theta$ and $\tau_{R\theta}$ are the radial displacement, horizontal normal stress, vertical normal stress and shear stress at the point $q(R,0,\theta)$ of the polar coordinate system in the infinite soil mass,

respectively; $\theta$ is the angle from $x$ axis direction to $R$ direction in the plane rectangular coordinate system.

According to the above theory and linear elastic superposition principle [7], when the boundary effect of horizontal and vertical ground surfaces is not considered, the elastic solutions of displacements at the point $q(x,0,z)$ in infinite soil mass under the common action of the real source and mirror source are expected as follows:

$$U_{x1}=U_{R1}\cos\theta_1+U_{R2}\cos\theta_2=\frac{pr_0{}^2}{2G}\Big(\frac{x+t}{R_1{}^2}+\frac{x-t}{R_2{}^2}\Big), \tag{2.5a}$$

$$U_{z1}=U_{R1}\sin\theta_1+U_{R2}\sin\theta_2=\frac{pr_0{}^2}{2G}\Big(\frac{z-h}{R_1^2}+\frac{z-h}{R_2^2}\Big), \tag{2.5b}$$

$$U_1=\sqrt{U_{x1}{}^2+U_{z1}{}^2}, \tag{2.5c}$$

where, $U_{x1}$, $U_{z1}$ and $U_1$ are the unrevised horizontal, vertical and total displacement at the point $q(x,0,z)$ of the space rectangular coordinate system under the vertical non-axisymmetric displacement boundary condition, respectively; $\theta_1$ and $\theta_2$ are the angle from x axis direction to $R_1$ direction and $R_2$ direction in the space rectangular coordinate system, respectively.

Similarly, because the problem studied in this paper can be regarded as a plane strain problem, the stress solutions at the point $q(x,0,z)$ are shown as follows:

$$\begin{aligned}\sigma_{x1}&=\big(\sigma_{R_1}\cos^2\theta_1+\sigma_{\theta_1}\sin^2\theta_1-\tau_{R\theta_1}\sin2\theta_1\big)+\big(\sigma_{R_2}\cos^2\theta_2+\sigma_{\theta_2}\sin^2\theta_2-\tau_{R\theta_2}\sin2\theta_2\big)\\&=pr_0{}^2\Big[\frac{1}{R_1^2}-\frac{2(x+t)^2}{R_1^4}+\frac{1}{R_2^2}-\frac{2(x-t)^2}{R_2^4}\Big],\end{aligned} \tag{2.6a}$$

$$\begin{aligned}\sigma_{z1}&=\big(\sigma_{R_1}\sin^2\theta_1+\sigma_{\theta_1}\cos^2\theta_1+\tau_{R\theta_1}\sin2\theta_1\big)+\big(\sigma_{R_2}\sin^2\theta_2+\sigma_{\theta_2}\cos^2\theta_2+\tau_{R\theta_2}\sin2\theta_2\big)\\&=pr_0{}^2\Big[\frac{1}{R_1^2}-\frac{2(z-h)^2}{R_1^4}+\frac{1}{R_2^2}-\frac{2(z-h)^2}{R_2^4}\Big],\end{aligned} \tag{2.6b}$$

$$\sigma_{y1}=v(\sigma_{x1}+\sigma_{z1})=0, \tag{2.6c}$$

$$\begin{aligned}\tau_{xz1}&=[(\sigma_{R_1}-\sigma_{\theta_1})\sin\theta_1\cos\theta_1+\tau_{R\theta_1}\cos2\theta_1]+[(\sigma_{R2}-\sigma_{\theta2})\sin\theta_2\cos\theta_2+\tau_{R\theta_2}\cos2\theta_2]\\&=-2pr_0{}^2\Big[\frac{(x+t)(z-h)}{R_1^4}+\frac{(x-t)(z-h)}{R_2^4}\Big],\end{aligned} \tag{2.6d}$$

where, $\sigma_{x1}$, $\sigma_{y1}$, $\sigma_{z1}$ and $\tau_{xz1}$ are the unrevised horizontal normal stress, axial normal stress, vertical normal stress, and shear stress at the point $q(x,0,z)$ of the space rectangular coordinate system under the vertical non-axisymmetric displacement boundary condition, respectively.

Due to the combination action of the cylindrical cavity expansion source and image source, the vertical normal stress and shear stress on the horizontal ground surface boundary (i.e., $z=0$) are respectively given by substituting $z=0$ into Eq. (2.6b) and

Eq. (2.6d) as follows:

$$\sigma_{z1}\big|_{z=0}=pr_0{}^2\left\{\frac{(x+t)^2-h^2}{\left[(x+t)^2+h^2\right]^2}+\frac{(x-t)^2-h^2}{\left[(x-t)^2+h^2\right]^2}\right\}\neq 0, \tag{2.7a}$$

$$\tau_{xz1}\big|_{z=0}=2pr_0{}^2\left\{\frac{(x+t)h}{\left[(x+t)^2+h^2\right]^2}+\frac{(x-t)h}{\left[(x-t)^2+h^2\right]^2}\right\}\neq 0. \tag{2.7b}$$

Moreover, because of the combined action of the cylindrical cavity expansion source and image source, the horizontal normal stress and shear stress on the vertical surface (i.e., $z=0$) are respectively expressed by substituting $z=0$ into Eq. (2.6a) and Eq. (2.6d) as follows:

$$\sigma_{x1}\big|_{x=0}=\frac{2pr_0{}^2[(z-h)^2-t^2]}{\left[t^2+(z-h)^2\right]^2}\neq 0, \tag{2.8a}$$

$$\tau_{xz1}\big|_{x=0}=0. \tag{2.8b}$$

It can be known from the Eq. (2.7a) and Eq. (2.7b) that the vertical normal stress and shear stress, which do not satisfy the condition of the free displacement boundary, are produced in the horizontal ground surface boundary. Likewise, it can be also found from the Eq. (2.8a) and Eq. (2.8b) that the horizontal normal stress, which does not satisfy the condition of the free displacement boundary, is produced in the vertical surface boundary. In order to satisfy the boundary stress condition, two stress correction processes are used to modify the vertical normal stress and shear stress of the horizontal ground surface. The horizontal normal stress of the vertical surface boundary is corrected by the means of the Boussinesq's solution and the integrating idea.

### 2.4.2 Correction of the vertical normal stress on the horizontal ground surface boundary

As shown in Fig. 4, to revise the vertical normal stress of the ground surface boundary to be zero, the equivalent vertical normal stress with the opposite direction and zero shear stress are applied to the ground surface boundary (i.e., $\sigma_{z2}|_{z=0}=-\sigma_{z1}|_{z=0}$ and $\tau_{xz2}|_{z=0}=0$). The stress function solutions [4] are used to obtain the revised stress and displacement on the ground surface boundary and expressed as follows:

$$U_{x2}=(1-2v)\frac{\partial f}{\partial x}+z\frac{\partial^2 f}{\partial x\partial z}, \tag{2.9a}$$

$$U_{z2}=-2(1-v)\frac{\partial f}{\partial z}+z\frac{\partial^2 f}{\partial z^2}, \tag{2.9b}$$

$$U_2=\sqrt{U_{x2}{}^2+U_{z2}{}^2}, \tag{2.9c}$$

$$\sigma_{x2}=2G\Big[(1-2v)\frac{\partial^2 f}{\partial x^2}-2v\frac{\partial^2 f}{\partial z^2}+z\frac{\partial^3 f}{\partial x^2\partial z}\Big], \tag{2.9d}$$

$$\sigma_{y2}=2G\Big[\frac{1}{x}\frac{\partial f}{\partial x}+2v\frac{\partial^2 f}{\partial x^2}+\frac{z}{x}\frac{\partial^2 f}{\partial x\partial z}\Big], \tag{2.9e}$$

$$\sigma_{z2}=2G\Big[-\frac{\partial^2 f}{\partial z^2}+z\frac{\partial^3 f}{\partial x^2\partial z}\Big], \tag{2.9f}$$

$$\tau_{zx2}=\tau_{xz2}=2Gz\frac{\partial^3 f}{\partial x\partial z^2}. \tag{2.9g}$$

The improved stress harmonic function is defined as follows:

$$f=A(\ln R_3+\ln R_4), \tag{2.10}$$

where, $A$ is an undetermined constant, which can be solved by the condition that the vertical normal stress is zero on the horizontal ground surface. $R_3$ and $R_4$ can be, respectively, expressed as:

$$\begin{cases} R_3=\sqrt{(x+t)^2+(z+h)^2}, \\ R_4=\sqrt{(x-t)^2+(z+h)^2}, \end{cases} \tag{2.11}$$

where, $R_3$ is the distance between the symmetrical position of the horizontal ground surface at the center of cylindrical cavity expansion source and the calculation point $q(x,0,z)$. $R_4$ is the distance between the symmetrical position of the horizontal ground surface at the center of image source and the calculation point $q(x,0,z)$.

The solutions for the vertical normal stress, which are on the horizontal ground surface boundary ($z$=0) in the first stress correction process, are obtained by solving Eq. (2.9f)

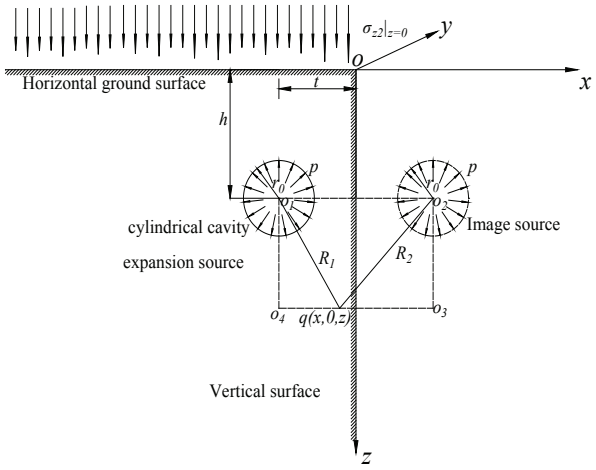


Figure 4: The vertical normal stress correction on the horizontal ground surface boundary.

by the condition of $\nabla^2 f=0$,

$$\sigma_{z2}|_{z=0}=-2GA\left\{\frac{(x+t)^2-h^2}{\left[(x+t)^2+h^2\right]^2}+\frac{(x-t)^2-h^2}{\left[(x-t)^2+h^2\right]^2}\right\}. \tag{2.12}$$

As zero value of the vertical normal stress is a necessary condition for the free ground surface boundary, zero value for the vertical normal stress of the ground surface boundary is induced by the cylindrical cavity expansion if the suitable constant $A$ is obtained (i.e., $\sigma_{z2}|_{z=0}=-\sigma_{z1}|_{z=0}$). Combining Eqs. (2.7a) and (2.12), it results in

$$\begin{aligned}&-2GA\left\{\frac{(x+t)^2-h^2}{\left[(x+t)^2+h^2\right]^2}+\frac{(x-t)^2-h^2}{\left[(x-t)^2+h^2\right]^2}\right\}\\&=-{pr_0}^2\left\{\frac{(x+t)^2-h^2}{\left[(x+t)^2+h^2\right]^2}+\frac{(x-t)^2-h^2}{\left[(x-t)^2+h^2\right]^2}\right\}.\end{aligned} \tag{2.13}$$

By solving Eq. (2.9e), the following expression is obtained:

$$A=\frac{pr_0^2}{2G}. \tag{2.14}$$

By substituting Eq. (2.14) into Eq. (2.9a) to Eq. (2.9g), displacements and stresses during the revision process of the vertical normal stress are obtained by

$$U_{x2}=\frac{pr_0^2}{2G}\Big[\frac{(1-2v)(x+t)}{R_3^2}-\frac{2z(x+t)(z+h)}{R_3^4}+\frac{(1-2v)(x-t)}{R_4^2}-\frac{2z(x-t)(z+h)}{R_4^4}\Big], \tag{2.15a}$$

$$vU_{z2}=\frac{pr_0^2}{2G}\Big[\frac{-2(1-v)(z+h)}{R_3^2}+\frac{z}{R_3^2}-\frac{2z(z+h)^2}{R_3^4}+\frac{-2(1-v)(z+h)}{R_4^2}+\frac{z}{R_4^2}-\frac{2z(z+h)^2}{R_4^4}\Big], \tag{2.15b}$$

$$U_2=\sqrt{{U_{x2}}^2+{U_{z2}}^2}, \tag{2.15c}$$

$$\sigma_{x2}=pr_0^2\Big[\frac{1-4v}{R_3^2}-\frac{2z(z+h)}{R_3^4}+\frac{8(x+t)^2z(z+h)}{R_3^6}+\frac{1-4v}{R_4^2}-\frac{2z(z+h)}{R_4^4}+\frac{8(x-t)^2z(z+h)}{R_4^6}\Big], \tag{2.15d}$$

$$\begin{aligned}\sigma_{y2}=pr_0^2\Big[&\frac{x+t}{xR_3^2}+\frac{2v}{R_3^2}-\frac{4v(x+t)^2}{R_3^4}-\frac{2(x+t)z(z+h)}{R_3^4}+\frac{x-t}{xR_4^2}+\frac{2v}{R_4^2}\\&-\frac{4v(x-t)^2}{R_4^4}-\frac{2(x-t)z(z+h)}{R_4^4}\Big],\end{aligned} \tag{2.15e}$$

$$\begin{aligned}\sigma_{z2}=pr_0^2\Big[&-\frac{1}{R_3^2}+\frac{2(z+h)^2-6z(z+h)}{R_3^4}+\frac{8z(z+h)^3}{R_3^6}\\&-\frac{1}{R_4^2}+\frac{2(z+h)^2-6z(z+h)}{R_4^4}+\frac{8z(z+h)^3}{R_4^6}\Big],\end{aligned} \tag{2.15f}$$

$$\tau_{xz2}=pr_0^2\Big[-\frac{2(x+t)z}{R_3^4}+\frac{8(x+t)(z+h)^2z}{R_3^6}-\frac{2(x-t)z}{R_4^4}+\frac{8(x-t)(z+h)^2z}{R_4^6}\Big]. \tag{2.15g}$$

### 2.4.3 Correction of shear stress on the horizontal ground surface boundary

As shown in Fig. 5, to correct the shear stress of the horizontal ground surface boundary to be zero, the equivalent shear stress with the opposite direction and zero value of the vertical normal stress are applied to the ground surface boundary (i.e., $\tau_{xz3}|_{z=0}=-\tau_{xz1}|_{z=0}$ and $\tau_{xz3}|_{z=0}=-\tau_{xz1}|_{z=0}$) The stress function solutions [4] can be applied to obtain the revised displacements and stresses and expressed as follows:

$$U_{x3}=2(1-v)\frac{\partial g}{\partial x}+z\frac{\partial^2 g}{\partial x\partial z}, \tag{2.16a}$$

$$U_{z3}=-(1-2v)\frac{\partial g}{\partial z}+z\frac{\partial^2 g}{\partial z^2}, \tag{2.16b}$$

$$U_3=\sqrt{{U_{x3}}^2+{U_{z3}}^2}, \tag{2.16c}$$

$$\sigma_{x3}=2G\Big[2\frac{\partial^2 g}{\partial x^2}-\frac{2v}{x}\frac{\partial g}{\partial x}+z\frac{\partial^3 g}{\partial x^2\partial z}\Big], \tag{2.16d}$$

$$\sigma_{y3}=2G\Big[\frac{1}{x}\frac{\partial g}{\partial x}+2v\frac{\partial^2 g}{\partial x^2}+\frac{z}{x}\frac{\partial^2 g}{\partial x\partial z}\Big], \tag{2.16e}$$

$$\sigma_{z3}=2Gz\frac{\partial^3 g}{\partial z^3}, \tag{2.16f}$$

$$\tau_{xz3}=\tau_{xz3}=2G\Big[\frac{\partial^2 g}{\partial x\partial z}+z\frac{\partial^3 g}{\partial x\partial z^2}\Big]. \tag{2.16g}$$

The improved stress harmonic function is defined as:

$$g=B(\ln R_3+\ln R_4), \tag{2.17}$$

where, $B$ is an undetermined constant, which can be calculated by the condition that the shear stress of horizontal ground surface is equal to zero.

In order to satisfy the harmonic equation ($\nabla^2 g=0$), based on Eq. (2.16g), the shear stress on the horizontal ground surface boundary ($z=0$) in the second stress revision are obtain by

$$\tau_{xz3}|_{z=0}=-4GB\left\{\frac{(x+t)h}{\left[(x+t)^2+h^2\right]^2}+\frac{(x-t)h}{\left[(x-t)^2+h^2\right]^2}\right\}. \tag{2.18}$$

Because the shear stress of the free surface displacement boundary must be equal to zero in this paper, resulting from the cylindrical cavity expansion, the shear stress of the horizontal ground surface boundary can only be balanced by the determination of the suitable constant $B$ (i.e., $\tau_{zx3}|_{z=0}=-\tau_{zx1}|_{z=0}$). Combining Eqs. (2.7b) and (2.18), it leads to

$$\begin{aligned}&-4GB\left\{\frac{(x+t)h}{\left[(x+t)^2+h^2\right]^2}+\frac{(x-t)h}{\left[(x-t)^2+h^2\right]^2}\right\}\\&=-2p{r_0}^2\left\{\frac{(x+t)\cdot h}{\left[(x+t)^2+h^2\right]^2}+\frac{(x-t)h}{\left[(x-t)^2+h^2\right]^2}\right\}.\end{aligned} \tag{2.19}$$

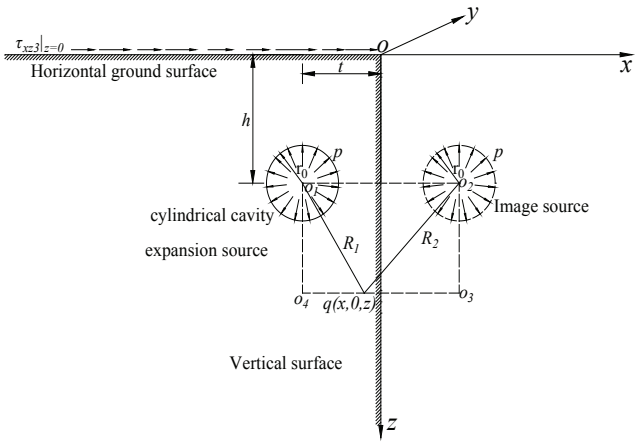


Figure 5: Shear stress correction on the horizontal ground surface boundary.

By solving Eq. (2.19), it results in

$$B=\frac{pr_0^2}{2G}. \tag{2.20}$$

By substituting Eq. (2.20) into Eq. (2.16a) to Eq. (2.16g), displacement and stress during the correction process of shear stress can be expressed as follows:

$$U_{x3}=\frac{pr_0^2}{2G}\Big[\frac{2(1-v)(x+t)}{R_3^2}-\frac{2z(x+t)(z+h)}{R_3^4}+\frac{2(1-v)(x-t)}{R_4^2}-\frac{2z(x-t)(z+h)}{R_4^4}\Big], \tag{2.21a}$$

$$U_{z3}=\frac{pr_0^2}{2G}\Big[\frac{-(1-2v)(z+h)}{R_3^2}+\frac{z}{R_3^2}-\frac{2z(z+h)^2}{R_3^4}+\frac{-(1-2v)(z+h)}{R_4^2}+\frac{z}{R_4^2}-\frac{2z(z+h)^2}{R_4^4}\Big], \tag{2.21b}$$

$$U_3=\sqrt{{U_{x3}}^2+{U_{z3}}^2}, \tag{2.21c}$$

$$\begin{aligned}\sigma_{x3}=pr_0^2\Big[&\frac{2}{R_3^2}-\frac{4(x+t)^2}{R_3^4}-\frac{2v(x+t)}{xR_3^2}-\frac{2z(z+h)}{R_3^4}+\frac{8(x+t)^2z(z+h)}{R_3^6}+\frac{2}{R_4^2}\\&-\frac{4(x-t)^2}{R_4^4}-\frac{2v(x-t)}{xR_4^2}-\frac{2z(z+h)}{R_4^4}+\frac{8(x-t)^2z(z+h)}{R_4^6}\Big],\end{aligned} \tag{2.21d}$$

$$\begin{aligned}\sigma_{y3}=pr_0^2\Big[&\frac{x+t}{xR_3^2}+\frac{2v}{R_3^2}-\frac{4v(x+t)^2}{R_3^4}-\frac{2(x+t)z(z+h)}{R_3^4}+\frac{x-t}{xR_4^2}\\&+\frac{2v}{R_4^2}-\frac{4v(x-t)^2}{R_4^4}-\frac{2(x-t)z(z+h)}{R_4^4}\Big],\end{aligned} \tag{2.21e}$$

$$\sigma_{z3}=pr_0^2\Big[\frac{8z(z+h)^3}{R_3^6}-\frac{6z(z+h)^2}{R_3^2}+\frac{8z(z+h)^3}{R_4^6}-\frac{6z(z+h)^2}{R_4^2}\Big], \tag{2.21f}$$

$$\tau_{xz3}=pr_0^2\Big[-\frac{2(x+t)(z+h)}{R_3^4}+\frac{-2(x+t)z}{R_3^4}+\frac{8(x+t)(z+h)^2z}{R_3^6}$$
$$-\frac{2(x-t)(z+h)}{R_4^4}+\frac{-2(x-t)z}{R_4^4}+\frac{8(x-t)(z+h)^2z}{R_4^6}\Big]. \tag{2.21g}$$

### 2.4.4 Correction of the horizontal normal stress on the vertical surface boundary

As shown in Fig. 6, it can be known that zero value of the shear stress and equivalent horizontal normal stress with the opposite direction are generated under the combination action of the cylinder cavity expansion source and image source. The following solutions are adopted to correct the horizontal normal stress of the vertical surface boundary in order to satisfy the condition of the free vertical surface boundary.

Because the equivalent normal stress with the opposite direction (i.e., $\sigma_{x2}|_{x=0}=-\sigma_{x1}|_{x=0}$) is applied to the stress correction of vertical surface boundary, the expression of the applied horizontal normal stress can be concluded by Eq. (2.8b) as follows:

$$\sigma_{x2}|_{x=0}=\sigma(\rho)=\frac{2p{r_0}^2[t^2-(\rho-h)^2]}{\left[t^2+(\rho-h)^2\right]^2}, \tag{2.22}$$

where, $\rho$ is the vertical coordinate of non-uniform distributed force, whose range is $(0,10h)$.

In order to satisfy the boundary condition of zero value of the horizontal normal stress on the vertical ground surface boundary, the stress correction of the vertical surface boundary can be obtained by the Boussinesq's solution [1] and the internal method. There is the elastic solution of the semi-infinite space which suffers from the normal con-

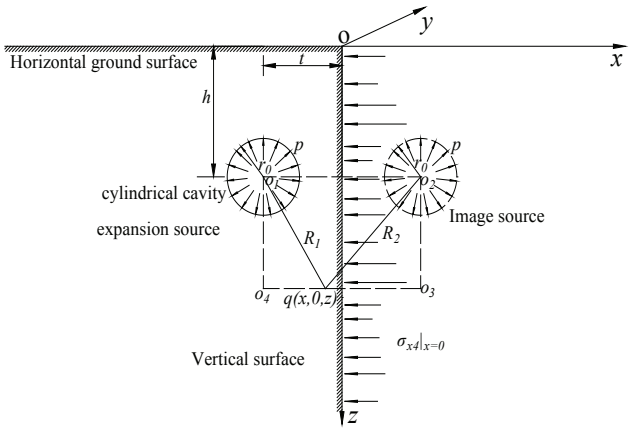


Figure 6: Horizontal normal stress correction on the vertical surface boundary.

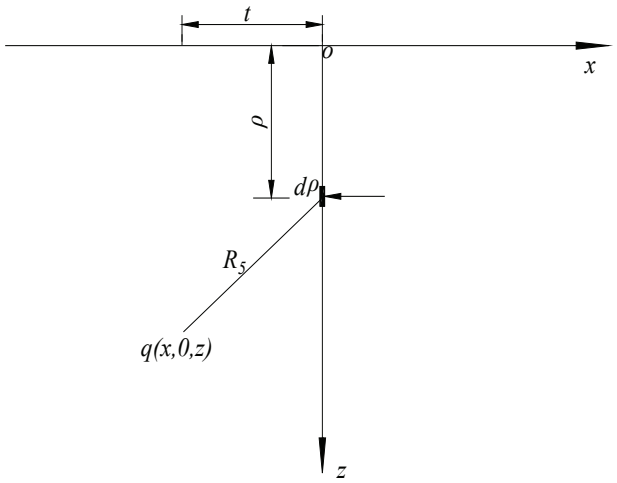


Figure 7: Horizontal normal stress calculation of the vertical ground surface boundary.

centrated force action as follows:

$$U_x = \frac{(1+\mu)P}{2\pi ER}\left[\frac{xz}{R^2} - \frac{(1-2\mu)x}{R+z}\right], \tag{2.23a}$$

$$U_z = \frac{(1+\mu)P}{2\pi ER}\left[2(1-\mu) + \frac{z^2}{R^2}\right], \tag{2.23b}$$

$$U = \sqrt{{U_x}^2 + {U_z}^2}, \tag{2.23c}$$

$$\sigma_x = \frac{P}{2\pi R^2}\left[\frac{(1-2\mu)R}{R+z} - \frac{3x^2z}{R^3}\right], \tag{2.23d}$$

$$\sigma_y = \frac{(1-2\mu)P}{2\pi R^2}\left(\frac{z}{R} - \frac{R}{R+z}\right), \tag{2.23e}$$

$$\sigma_z = -\frac{3Pz^3}{2\pi R^5}, \tag{2.23f}$$

$$\tau_{xz} = \tau_{zx} = -\frac{3Pxz^2}{2\pi R^5}. \tag{2.23g}$$

The stress and displacement at the calculation point $q(x,0,z)$, resulting from the non-uniform horizontal distributed force, will be solved by the means of the integral method. The specific solving steps are as follows.

As shown in Fig. 7, the non-uniform distributed force $\sigma_{x2}|_{x=0}$ acts on the vertical ground surface boundary. The line micro unit is determined in the range of the horizontal distributed force ($dA' = d\rho'$), where $\rho'$ is the radius coordinate of the unit. Therefore, the horizontal distributed force on the micro unit can be expressed as $dq' = \sigma(\rho')d\rho'$.

Displacements and stresses of line micro unit, which are generated by the Boussi-

nesq's solution [1], can be given as follows:

$$dU_{x4}=\frac{(1+v)}{2\pi ER_5}\Big[\frac{xz}{{R_5}^2}-\frac{(1-2v)x}{R_5+z}\Big]dq, \tag{2.24a}$$

$$dU_{z4}=\frac{(1+v)}{2\pi ER_5}\Big[2(1-v)+\frac{z^2}{{R_5}^2}\Big]dq, \tag{2.24b}$$

$$d\sigma_{x4}=\frac{1}{2\pi {R_5}^2}\Big[\frac{(1-2v)R_7}{R_5+z}-\frac{3x'^2z}{{R_5}^3}\Big]dq, \tag{2.24c}$$

$$d\sigma_{y4}=\frac{(1-2v)}{2\pi {R_5}^2}\Big(\frac{z}{R_5}-\frac{R_7}{R_5+z}\Big)dq, \tag{2.24d}$$

$$d\sigma_{z4}=-\frac{3z^3}{2\pi {R_5}^5}dq, \tag{2.24e}$$

$$d\tau_{zx4}=d\tau_{xz4}=-\frac{3xz^2}{2\pi {R_5}^5}dq. \tag{2.24f}$$

Displacements and stresses at the point $q(x',0,z')$, which are generated by the non-uniform horizontal distributed force, can be solved by the integral method as follows:

$$U_{x4}=\int_0^{10h}\frac{(1+v)}{2\pi ER_5}\Big[\frac{xz}{{R_5}^2}-\frac{(1-2v)x}{R_5+z}\Big]\left\{\frac{2p{r_0}^2[t^2-(\rho-h)^2]}{\big[t^2+(\rho-h)^2\big]^2}\right\}d\rho, \tag{2.25a}$$

$$U_{z4}=\int_0^{10h}\frac{(1+v)}{2\pi ER_5}\left[2(1-v)+\frac{z^2}{{R_5}^2}\right]\left\{\frac{2p{r_0}^2[t^2-(\rho-h)^2]}{\big[t^2+(\rho-h)^2\big]^2}\right\}d\rho, \tag{2.25b}$$

$$U_4=\sqrt{{U_{x4}}^2+{U_{z4}}^2}, \tag{2.25c}$$

$$\sigma_{x4}=\int_0^{10h}\frac{1}{2\pi {R_5}^2}\left[\frac{(1-2v)R_5}{R_5+z}-\frac{3x^2z}{{R_5}^3}\right]\left\{\frac{2p{r_0}^2[t^2-(\rho-h)^2]}{\big[t^2+(\rho-h)^2\big]^2}\right\}d\rho, \tag{2.25d}$$

$$\sigma_{y4}=\int_0^{10h}\frac{(1-2v)}{2\pi {R_5}^2}\left(\frac{z}{R_5}-\frac{R_5}{R_5+z}\right)\left\{\frac{2p{r_0}^2[t^2-(\rho-h)^2]}{\big[t^2+(\rho-h)^2\big]^2}\right\}d\rho, \tag{2.25e}$$

$$\sigma_{z4}=\int_0^{10h}\left(-\frac{3z^3}{2\pi {R_5}^5}\right)\left\{\frac{2p{r_0}^2[t^2-(\rho-h)^2]}{\big[t^2+(\rho-h)^2\big]^2}\right\}d\rho, \tag{2.25f}$$

$$\tau_{xz4}=\int_0^{10h}\left(-\frac{3xz^2}{2\pi {R_5}^5}\right)\left\{\frac{2p{r_0}^2[t^2-(\rho-h)^2]}{\big[t^2+(\rho-h)^2\big]^2}\right\}d\rho, \tag{2.25g}$$

where, $R_5$ is the distance between the calculation point $q(x',0,z')$ and the loading position (i.e., $R_5=\sqrt{x^2+(z-\rho)^2}$). $U_{x4}$, $U_{z'4}$ are the modified horizontal and vertical displacements on the vertical surface boundary, respectively. $\sigma_{x4}$, $\sigma_{y4}$, $\sigma_{z4}$ and $\tau_{xz4}$ are the revised horizontal normal stress, axis normal stress, vertical normal stress and shear stress on the vertical ground surface boundary, respectively.

### 2.4.5 Elastic solution after correction

Based on the linear elastic superposition principle [7] and the combination of Eqs. (2.5a)-(2.6d), (2.15a)-(2.15g), (2.21a)-(2.21g) and (2.25a)-(2.25g), the elastic solutions of displacement and stress at the calculation point $q(x,0,z)$ under vertical non-axisymmetric displacement boundary condition on vertical surface can be obtained by the linear superposition as follows.

$$U_x = U_{x1}+U_{x2}+U_{x3}+U_{x4}, \tag{2.26a}$$
$$U_z = U_{z1}+U_{z2}+U_{z3}+U_{z4}, \tag{2.26b}$$
$$U = U_1+U_2+U_3+U_4, \tag{2.26c}$$
$$\sigma_x = \sigma_{x1}+\sigma_{x2}+\sigma_{x3}+\sigma_{x4}, \tag{2.26d}$$
$$\sigma_y = \sigma_{y1}+\sigma_{y2}+\sigma_{y3}+\sigma_{y4}, \tag{2.26e}$$
$$\sigma_z = \sigma_{z1}+\sigma_{z2}+\sigma_{z3}+\sigma_{z4}, \tag{2.26f}$$
$$\tau_{xz} = \tau_{xz1}+\tau_{xz2}+\tau_{xz3}+\tau_{xz4}, \tag{2.26g}$$
$$\sigma = \sqrt{{\sigma_x}^2+{\sigma_y}^2+{\sigma_z}^2}. \tag{2.26h}$$

## 2.5 Maximum grouting pressure

Generally speaking, the horizontal ground surface settlement is emphasized on the shield tunnel construction. It can be known from Eq. (2.26b) that the vertical displacement of horizontal ground surface is given by

$$\begin{aligned} U_z|_{z=0} &= U_{z1}|_{z=0}+U_{z2}|_{z=0}+U_{z3}|_{z=0}+U_{z4}|_{z=0} \\ &= U_{z2}|_{z=0}+U_{z3}|_{z=0}+U_{z4}|_{z=0} \\ &= -\frac{4p{r_0}^2(1-v^2)h}{E}\Big[\frac{1}{(x+t)^2+h^2}+\frac{1}{(x-t)^2+h^2}\Big] \\ &\quad +\frac{2p{r_0}^2(1-v^2)}{\pi E}\int_0^{10h}\frac{t^2-(s-h)^2}{\big[t^2+(s-h)^2\big]^2\sqrt{x^2+s^2}}ds. \end{aligned} \tag{2.27}$$

The position of the maximum uplift for the ground surface should be located at the position $(x=-t)$, so the maximum vertical displacement is expressed as follows:

$$\begin{aligned} U_{z\max} &= -U_z(-t,0) \\ &= \frac{4p{r_0}^2(1-v^2)(4t^2+2h^2)}{Eh(4t^2+h^2)}-\frac{2p{r_0}^2(1-v^2)}{\pi E}\int_0^{10h}\frac{t^2-(s-h)^2}{\big[t^2+(s-h)^2\big]^2\sqrt{t^2+s^2}}ds. \end{aligned} \tag{2.28}$$

Because the complex integral is included in the Eq. (2.28), there will be much difficulty for the Eq. (2.28) in the shield tunnel application. In order to meet the convenience of the

formula and the requirement of the synchronous grouting of shield tunnel, Eq. (2.28) can be simplified and expressed as follows:

$$U_{z\max}=\frac{(p_g-p_0){r_0}^2(3-2v)(1+v)(4t^2+2h^2)}{Eh(4t^2+h^2)}, \tag{2.29}$$

where, $p_g$ is the grouting pressure, $p_0$ is the initial hydrostatic pressure of the stratum.

As we know, the maximum ground settlement is seen as the control parameter in the synchronous grouting of shield tunnel. Therefore, the maximum ground uplift formula caused by the synchronous grouting is given by the Eq. (2.29), which can provide some useful theoretical consultation for the surface subsidence control and the pressure setting of synchronous grouting. In addition, the maximum grouting pressure to control the ground uplift can be obtained by considering the initial hydrostatic pressure and identical transformation for the Eq. (2.30):

$$p_{\max}=p_0+\frac{Eh(4t^2+h^2)U_{z\max}}{{r_0}^2(3-2v)(1+v)(4t^2+2h^2)}. \tag{2.30}$$

Eq. (2.30) can be well applied in the stratum analysis of the synchronous grouting of shield tunnel in the shallow buried soft clay.

# 3 Numerical verification

In order to validate the correctness of the proposed approach, the displacement and stress solved by the proposed approach are compared with those of the numerical method. Displacement and stress of the soil mass on the right side of shield tunnel and the horizontal ground surface, and maximum uplift displacement on the horizontal ground surface are all carried out corresponding to $E=2.85$MPa, $v=0.5$, $p=0.06$MPa, $r_0=3.2$m, $h=8$m, $t=8$m (Ye et al., 2014). The specific comparison are shown in Figs. 8-11.

## 3.1 Displacements and stresses on the right side of shield tunnel

Displacements and stresses at point $q(-4.5,0,H)$ on the right side of shield tunnel calculated by the proposed approach and the numerical method under the vertical non-axisymmetric displacement boundary condition are shown in Fig. 8 and Fig. 9, respectively. Where, $H$ is the vertical coordinate of the right side of the shield tunnel.

As shown in Figs. 8 and 9, the variation regulations of the horizontal and vertical displacements, the horizontal normal stress, vertical normal stress and shear stress of the proposed approach agree well with those of the numerical method.

In addition, the difference of the horizontal displacement calculated by two methods is very small with the "$H$" increasing from 0 m to 20m, and the maximum value of horizontal displacement of the proposed approach is smaller than those of the numerical method by 6.91%. Moreover, the maximum horizontal normal stress, vertical normal

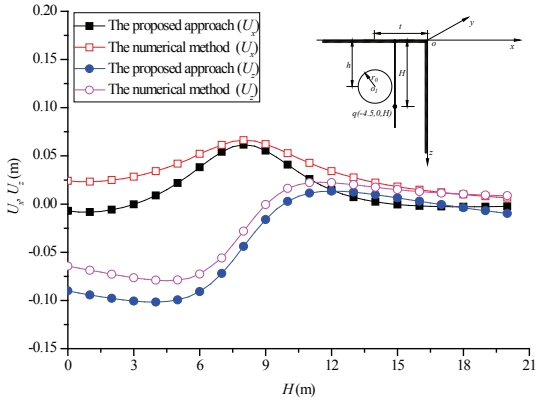


Figure 8: Displacements solved by the two methods on the right of shield tunnel.

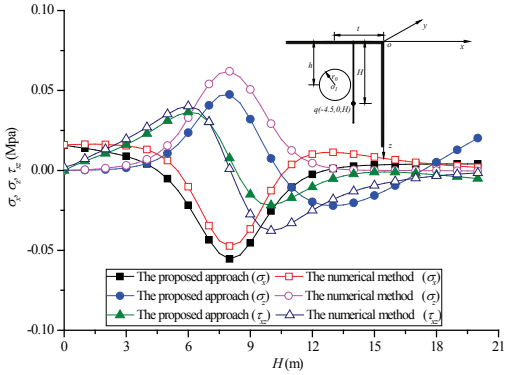


Figure 9: Stresses solved by two methods on the right of the shield tunnel.

stress, positive and negative shear stress of the proposed approach is larger than that of the numerical method by 16.7%, smaller than that of the numerical method by 25.4%, smaller than that of the numerical method by 5.91% and smaller than that of the numerical method by 41.1%, respectively. Therefore, the difference of the horizontal normal stress, vertical normal stress and shear stress solved by the two approaches can't be ignored with the soil mass depth increasing.

## 3.2 Displacements and stresses and on the horizontal ground surface boundary

Displacements and stresses at the point $q(D,0,0)$ of the horizontal ground surface calculated by the proposed approach and the numerical method under the vertical non-axisymmetric displacement boundary condition are shown in Figs. 10-11. Where, $D$ is the horizontal coordinate of the horizontal ground surface.

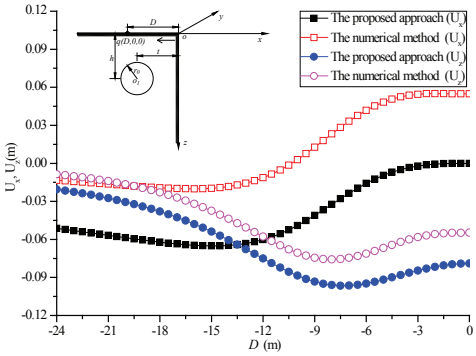


Figure 10: Displacements of the two methods on the horizontal ground surface boundary.

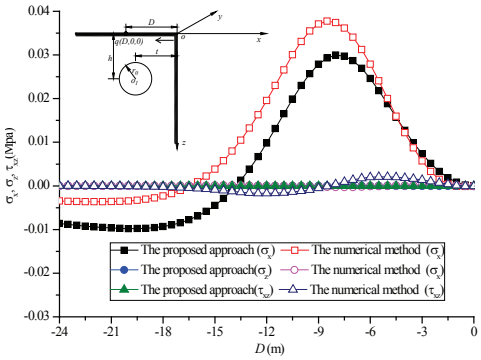


Figure 11: Stresses of the two methods on the horizontal ground surface boundary.

It can be found from Figs. 10-11 that the variation regulations of the horizontal and vertical displacements, the horizontal normal stress, vertical normal stress and shear stress of horizontal ground surface of the proposed approach agree well with those of the numerical method.

In addition, the difference of the horizontal and vertical displacement calculated by the proposed approach and the numerical method can't be ignored with the soil mass depth increasing, while the difference of the vertical normal stress and the shear stress, solved by the two approaches, can be ignored for the ground surface boundary. For example, the maximum horizontal and vertical displacements of horizontal ground surface of the numerical method are smaller than those of the proposed approach by 69.1% and 21.5%, respectively. The maximum horizontal normal stress of the proposed approach is smaller than that of the numerical method by 21.1%.

### 3.3 Maximum uplift displacement on the horizontal ground surface

The excavation radius of cutter head for the metro shield tunnel is 3.2m ($r_0 = 3.2$m), the shield tunnel depth is 10m ($h = 10$m), the limb distance is 12m ($t = 12$m), the elastic mod-

ulus of soils is 2.85MPa ($E=2.85$MPa), the soil Poisson's ratio is 0.5 ($v=0.5$), the initial hydrostatic pressure of surrounding soils is 0.24MPa ($p_0=0.24$MPa), the grouting pressure is 0.24MPa ($p_g=0.3$MPa).

Based on the above parameters, the maximum value of the horizontal ground surface calculated by the approach in Eq. (2.29), the numerical method and the proposed approach are 74.2mm, 58.1mm and 73.9mm, respectively. The difference of the uplift displacement on the ground surface between the results in Eq. (2.29) and the proposed approach is 0.41% ($e_{r1}=\frac{74.2-73.9}{73.9}\times 100\%=0.41\%$). The difference of the uplift displacement on the horizontal ground surface between the results in Eq. (2.29) and numerical method is 27.7% ($\frac{74.2-58.1}{58.1}\times 100\%=27.7\%$).

Therefore, the proposed approach of the uplift displacement on the horizontal ground surface in Eq. (2.29) is validated and can be satisfied the engineering practice under the non-axisymmetric displacement boundary condition on the vertical surface.

# 4 Numerical analysis and discussion

It can be known from Eq. (2.21f) to Eq. (2.25b) that displacements and stresses of the soil mass are mainly influenced by the tunnel depth and limb distance when the synchronous grouting of shield tunnel takes place under the vertical non-axisymmetric displacement boundary condition. Based on the parameters of numerical verification, the stresses and displacements on the right side of shield tunnel and vertical displacement of horizontal ground surface are selected to carry out the numerical analysis and discussion.

## 4.1 Effects of the shield tunnel depths on the stresses and displacements

To investigate the effect of the shield tunnel depth on the displacements and stresses of the soil mass on the right side of the tunnel, the revised and unrevised stresses and displacements with different tunnel depths (i.e., $h=8$m, 12m, 16m and 20m) at points $q(-8,0,H)$ are shown in Figs. 11 and 12 for $E=2.85$MPa, $v=0.5$, $p=0.06$MPa, $r_0=3.2$m and $t=12$m.

As is clearly shown in Figs. 12-13, the variation regulations of the unrevised and the revised results are similar for the horizontal normal stress, vertical normal stress, axial normal stress and shear stress, the horizontal and vertical displacements with the increase of the shield tunnel depth. However, when the shield tunnel depths are 8 meters, 12m, 16m and 20m, the revised results of the maximum shear stresses in the positive direction are larger than the unrevised results by 12.2%, 5.48%, 5.44% and 8.38%, respectively. In addition, when the shield tunnel depths are 8m, 12m, 16m and 20m, the revised results of the maximum horizontal and vertical displacement are smaller than the unrevised results by 11.1%, 3.17%, 1.21% and 1.22% and larger than the unrevised by 94.5%, 77.3%, 64.9% and 53.9%, respectively.

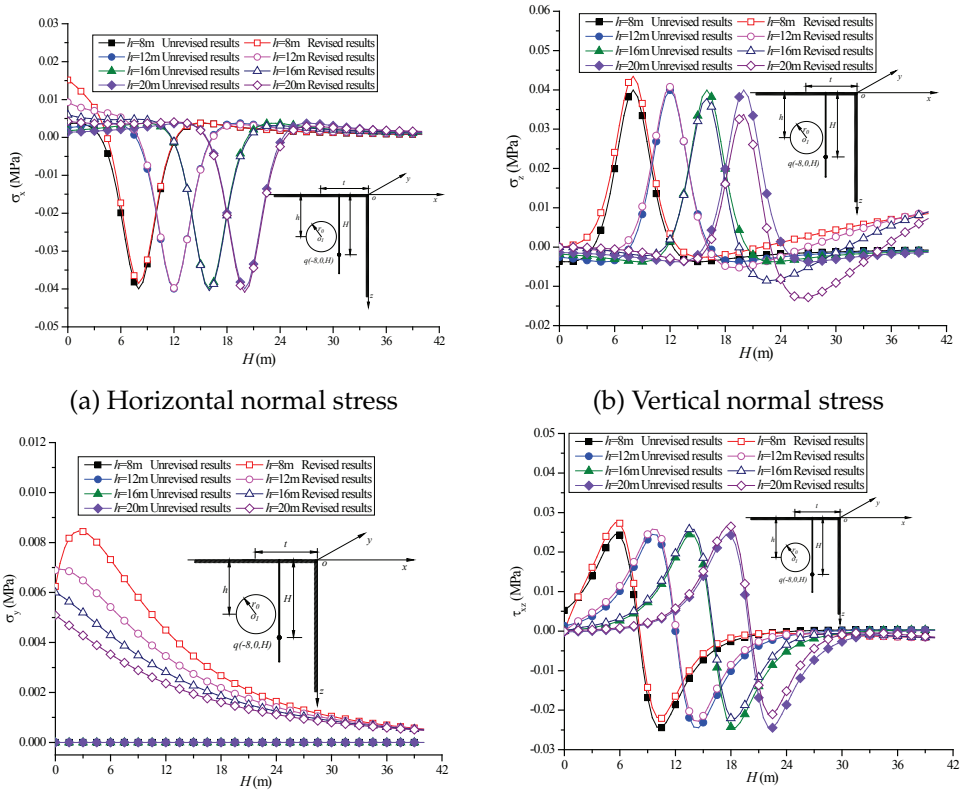


(a) Horizontal normal stress (b) Vertical normal stress

(c) Axial normal stress (d) Shear stress

Figure 12: Effects of the shield tunnel depth on the unrevised and revised stresses on the right side of shield tunnel.

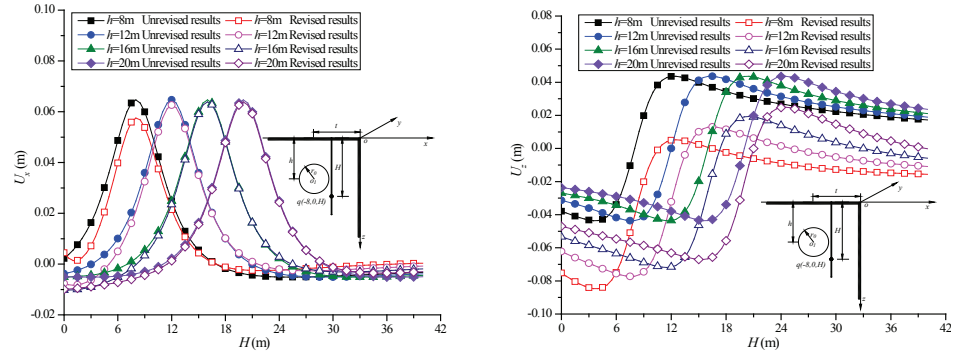


(a) Horizontal displacement (b) Vertical displacement

Figure 13: Effects of shield tunnel depth on the unrevised and revised displacements on the right side of shield tunnel.

## 4.2 Effects of the limb distances on the stresses and displacements

To investigate the influence of different limb distances on the displacement of the soil mass on the right side of the shield tunnel, the revised and unrevised stresses and displacements with different tunnel depths (i.e., $t=10$m, 12m, 14m and 16m) at point $q(-6,0,H)$ are shown in Figs. 13 and 14 for $E=2.85$MPa, $v=0.5$, $p=0.06$MPa, $r_0=3.2$m and $h=10$m.

It can be found from Figs. 14-15 that the variation regulations of the unrevised and revised results of horizontal normal stress, vertical normal stresses, axial normal stress and shear stress, the horizontal and vertical displacements calculated by the proposed approach. However, when the limb distances are 10m, 12m, 14m and 16m, the revised results of the maximum horizontal displacement are larger than the unrevised results by 0.49%, 2.43%, 39.8% and 15.2%, smaller than the unrevised results by 2.94%, 5.80%, 12.3% and 23.2% and larger than those of the unrevised results by 10.6%, 26.0%, 34.9% and 40.1%, respectively. Moreover, when the limb distances are 10m, 12m, 14m and 16m, the revised results of the maximum horizontal displacement are smaller than those of the

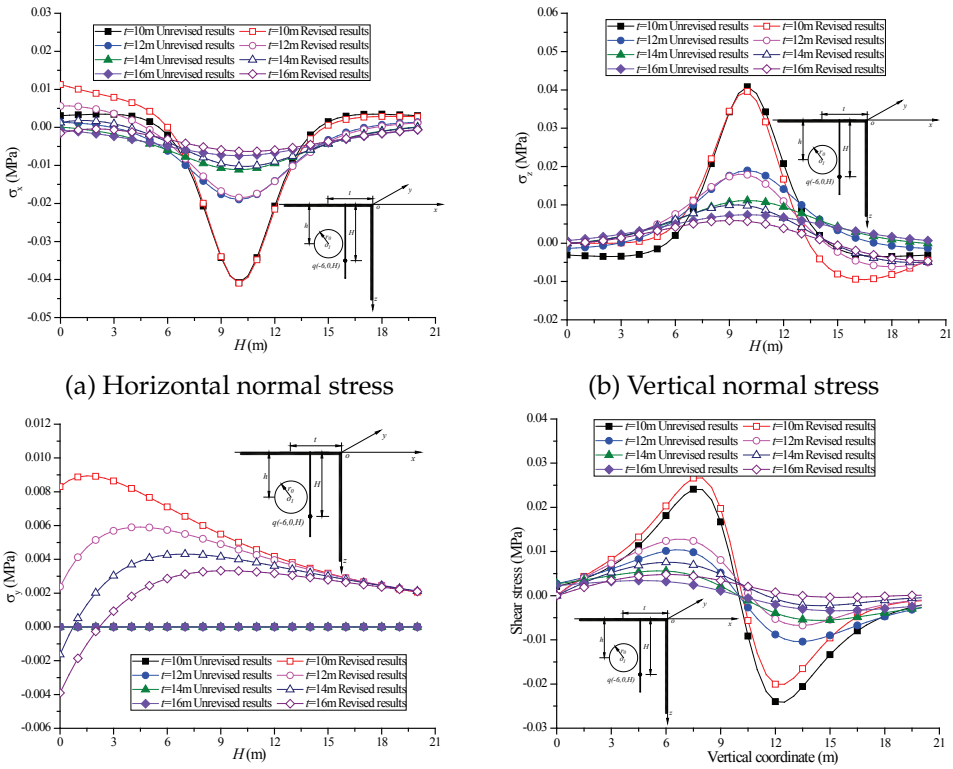


(a) Horizontal normal stress (b) Vertical normal stress

(c) Axial normal stress (d) Shear stress

Figure 14: Effects of the limb distance on the unrevised and revised stresses.

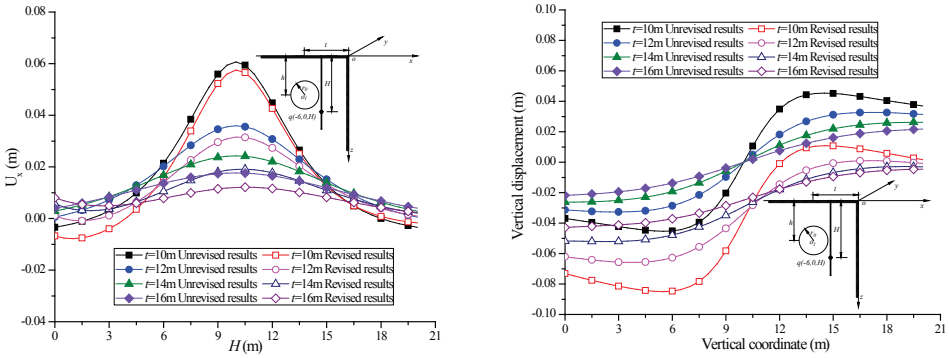


(a) Horizontal displacement (b) Vertical displacement

Figure 15: Effects of the limb distance on the unrevised and revised displacements.

unrevised results by 5.18%, 12.2%, 21.6% and 31.8% and larger than the unrevised results by 87.2%, 101.3%, 99.1% and 97.6%, respectively.

### 4.3 Effects of various influencing factors on the vertical displacement of horizontal ground surface

To investigate the effect of different tunnel depths, limb distances, internal expansion pressures, elastic modulus of soils and tunnel excavation radius on the vertical displacement of horizontal ground surface, the unrevised and revised results of the vertical displacement of horizontal ground surface with different shield tunnel depths (i.e., $h=10$m, 12m, 14m and 16m), limb distances (i.e., $t=10$m, 13m, 16m and 19m), internal expansion pressures (i.e., $p=0.01$MPa, 0.04MPa, 0.07MPa and 0.10MPa), elastic modulus of soils (i.e., $E=2.25$MPa, 2.50MPa, 2.75MPa and 3.00MPa) and tunnel excavation radius (i.e., $r_0=3.0$m, 3.5m, 4.0m and 4.5m) at the point $q(D,0,0)$ are shown in Figs. 16-20, where $D$ is the horizontal coordinate of the horizontal ground surface.

It can be known from Fig. 16 that the effect of the shield tunnel depth on the revised vertical displacement of horizontal ground surface decreases gradually with the increase of the shield tunnel depth, For example, when the shield tunnel depth increases from 8m to 20m by 4m, the revised result of the maximum vertical displacement of horizontal ground surface falls from 0.08844m to 0.04695m. And the decline range of the revised vertical displacement of horizontal ground surface falls from 27.0% to 12.1% when the shield depth increases from 8m to 20m by 4m.

It can be found from Fig. 17 that the revised vertical displacement of horizontal ground surface increases gradually with the limb distance increasing. For example, when the limb distance increases from 10m to 19m by 3m, the revised result of the maximum vertical displacement of horizontal ground surface increases from 0.07694m to 0.06861m. Moreover, the rise range of the revised vertical displacement of horizontal ground surface decreases from 5.50% to 2.20% when the limb distance increases from 10m to 19m by

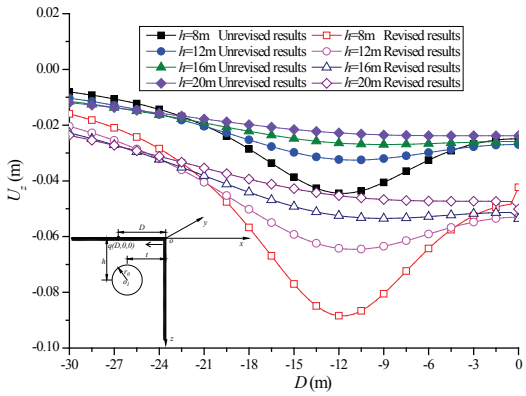


Figure 16: Effect of the shield tunnel depth on the vertical displacement of the horizontal ground surface.

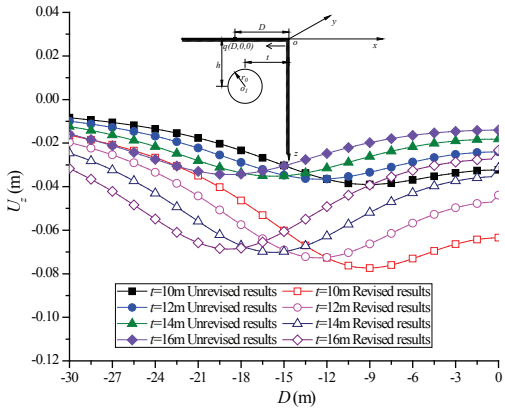


Figure 17: Effects of the limb distance on the vertical displacement the horizontal ground surface.

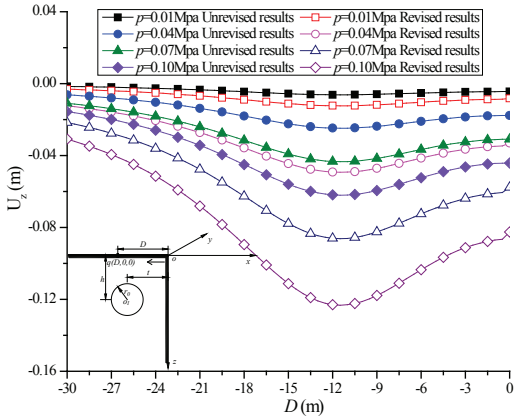


Figure 18: Effect of the internal expansion pressure on the vertical displacement of the horizontal ground surface.

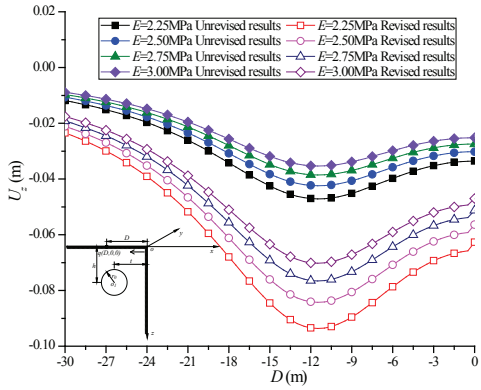


Figure 19: Effect of the elastic modules of soil on the vertical displacement of the horizontal ground surface.

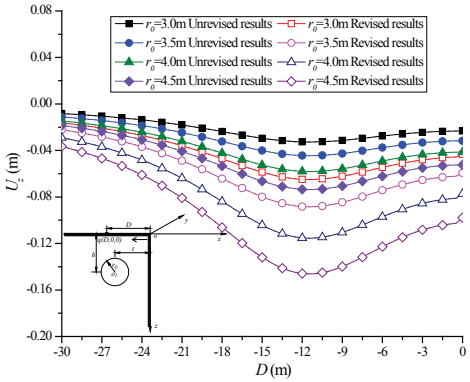


Figure 20: Effects of the shield tunnel excavation radius on the vertical displacement of the horizontal ground surface.

3m.

It can be known from Fig. 18 that the influence of the internal expansion pressure on the revised vertical displacement of horizontal ground surface weakens gradually with the expansion pressure increasing. For example, the rise range of the revised vertical displacement of horizontal ground surface decreases from 300% to 42.9% when the internal expansion pressure increases from 0.01MPa to 0.10MPa by 0.03MPa.

It can be found from Fig. 19 that the influence of the elastic modulus of soil mass on the revised vertical displacement of horizontal ground surface weakens gradually with the increase of the elastic modulus of soil. For instance, when the elastic modulus of soil increases from 2MPa to 3MPa by 0.25MPa, the decline range of the revised vertical displacement of horizontal ground surface decreases from 10.0% to 8.33%.

As is clearly shown in Fig. 20, the influence of the shield tunnel excavation radius on the revised vertical displacement of horizontal ground surface weakens gradually with the increase of the shield tunnel excavation radius. For instance, when the tunnel

excavation radius increases from 3.0m to 4.5m by 0.5m, the decline range of the revised vertical displacement of horizontal ground surface decreases from 10.0% to 8.33%.

In addition, the revised result of vertical displacement of horizontal ground surface corresponding to different shield tunnel depths, limb distances, expansion pressures, elastic modulus of soil and tunnel excavation radius is larger than that of the unrevised value by 100%.

## 5 Conclusions

This paper presents a new procedure for the synchronous grouting of shield tunnels under the vertical non-axisymmetric displacement boundary condition. Compared with the previous approach, the following improvements have been achieved.

(1) The stress function solutions are carried out to correct the vertical normal stress and the shear stress of horizontal ground surface boundary, the virtual image technique is applied to eliminate the shear stress of vertical ground surface boundary, and the Boussinesq's solution and the integral method were adopted to revise the horizontal normal stress of vertical ground surface boundary.

(2) The new approach for stresses, displacements and the maximum grouting pressure are based on the virtual image technique, improved stress harmonic function and Boussinesq's solution. The validity of the proposed approach was proved by the numerical results.

(3) The new approach extends method of the synchronous grouting of shield tunnels, particularly for the vertical non-axisymmetric displacement boundary condition, which could reflect the "boundary effect" of horizontal and vertical ground surface.

The new approach could form a theoretical basis for the synchronous grouting of shield tunnels, under the cavity contraction/expansion plane for the vertical non-axisymmetric displacement boundary condition.

## Acknowledgements

The authors are grateful to the Traffic Technology Fund of Guizhou Province of China (No. 2014-122-005) and the National Natural Science Foundation of China (Grant No. 51208523).

## References

[1] J. BOUSSINESQ, Application of Potentials in Balanced and Unbalanced Movement of Elastic Solides, Paris: Gauthier-Villars, 1885.

[2] R. B. PECK, *Deep excavations and tunneling in soft ground,* Proceedings of 7th International Conference on Soil Mechanics and Foundation Engineering, Mexico City, 1969.

[3] A. M. M. WOOD, *The circular tunnel in elastic ground,* Geotechnique, 25 (1975), pp. 115–127.

[4] M. K. KASSIR, G. C. SIH AND J. R. RICE, *Three-dimensional crack problems,* Mech Fract., 2 (1975), pp. 382–409.
[5] P. B. ATTEWELL AND J. P. WOODMAN, *Predicting the dynamics of ground settlement and its derivatives caused by tunneling in soil,* Ground. Eng., 15 (1982), pp. 13–22.
[6] C. SAGATASETA, *Analysis of undrained soil deformation due to ground loss,* Geotechnique., 37 (1987), pp. 301–320.
[7] R. O. DAVIS AND A. P. S. SELVADURAI, Elasticity and Geomechanics, London: Cambridge University Press, 1988.
[8] K. M. LEE, R. K. ROWE AND K. Y. LO, *Subsidence owing to tunneling I: estimating the gap parameter,* Can. Geotech. J., 29 (1992), pp. 929–940.
[9] R. K. ROWE AND K. M. LEE, *Subsidence owing to tunneling II: evaluation of a prediction technique,* Can. Geotech. J., 29 (1992), pp. 941–954.
[10] A. VREEUIJIT AND J. R. BOOKER, *Surface settlements due to deformation of a tunnel in an elastic half plane,* Geotechnique., 46 (1996), pp. 753–756.
[11] N. LOGANATHAN AND H. G. POULOS, *Analytical prediction for tunneling-induced ground movement in clays,* J. Geotech. Geoenviron. Eng., 124 (1998), pp. 846–856.
[12] G. SWOBODA AND A. ABU-KRISHA, *Three-dimensional numerical modeling for TBM tunneling in consolidated clay,* Tunn. Undergr. Space. Technol., 14 (1999), pp. 327–333.
[13] N. LOGANTHAN, H. G. POULOS AND D. P. STEWART, *Centrifuge testing of tunneling-induced ground and pile deformations,* Geotechnique., 50 (2000), pp. 283–294.
[14] J. P. BERG VAN DER, C. R. I. CLAYTON AND D. B. POWELL, *Displacements ahead of an advancing NATM tunnel in the London clay*, Geotechnique., 53 (2003), pp. 767–784.
[15] J. P. LI, Y. G. ZHANG, H. B. CHEN AND F. Y. LIANG, *Analytical solutions of spherical cavity expansion near a slope due to pile installation,* J. Appl. Math., 2013 (2013), pp. 1–11.
[16] F. YE, C. F. GOU, Z. CHEN, J. H. MAO, P. B. YANG AND T. JIA, *Ground surface deformation caused by synchronous grouting of Shield Tunnelling,* Yantu Gongcheng Xuebao, 36 (2014), pp. 618–624.
[17] J. F. ZOU AND S. S. LI, *Theoretical solution for displacement and stress in strain-softening surrounding rock under hydraulic-mechanical coupling,* Sci. China Tech. Sci., 58 (2015), pp. 1401–1413.
[18] J. F. ZOU AND Z. HE, *Numerical approach for strain-softening rock with axial stress,* Proc. Inst. Civ. Eng. Geotech. Eng., 169 (2016), pp. 276–290.
[19] J. F. ZOU, S. S. LI, Y. XU, H. C. DAN AND L. H. ZHAO, *Theoretical solution for a circular opening in an elastic-brittle-plastic rock mass incorporating the out-of-plane stress and seepage force*, KSCE J. Civ. Eng., 20 (2016), pp. 687–701.
[20] J. F. ZOU AND Y. SU, *Theoretical solutions of a circular tunnel with the influence of the out-of-plane stress based on the generalized HoekBrown failure criterion,* Int. J. Geomech., 16 (2016).
[21] J. F. ZOU AND S. Q. ZUO, *An approximate solution for the cylindrical cavity expansion under the non-axisymmetric displacement boundary condition on hypotenuse*, Int. J. Geotech. Eng., (2016), pp. 1–22.